J|A|C|S
ARTICLES
Published on Web 02/23/2007

Importance of Correlated Motions on the Low Barrier Rotational Potentials of Crystalline Molecular Gyroscopes

Peter D. Jarowski, K. N. Houk, and Miguel A. Garcia-Garibay*

Contribution from the Department of Chemistry and Biochemistry, University of California, Los Angeles, California 90095-1569

Received June 3, 2006; E-mail: edu

Abstract: The energetic and structural changes taking place upon rotation of the central phenylene of 1,4-bis(3,3,3-triphenylpropynyl)benzene in the solid state were computed using molecular mechanics calculations. Pseudopolymorphic crystals of a benzene clathrate (**1A**) and a desolvated form (**1B**) were analyzed with models that account for varying degrees of freedom within the corresponding lattices. The calculated rotational barriers in a rigid lattice approximation, 78 kcal/mol for **1A** and 72 kcal/mol for **1B**, are about 5 times greater than those previously measured by variable-temperature ^{13}C CPMAS NMR and quadrupolar echo ^{2}H NMR line-shape analysis: 12.8 kcal/mol for **1A** and 14.6 kcal/mol for **1B**. The potential energy barriers calculated with a model that restricts whole body rotation and translational motions but allows for internal rotations give results that are near the experimental free-energy barriers. The calculated barriers for **1A** and **1B** are 15.5 and 16.2 kcal/mol, respectively. The differences between the rigid and partially relaxed models are attributed to the effect of correlated motions of the lattice and the rotating group, which are evident from the structural analysis of the atomic position data as a function of the dihedral angle of the rotator. The displacements of neighboring molecules near the rotary transition states for **1A** and **1B** can be as large as 2.7 and 1.1 Å, respectively. The displacement and oscillation (C_2) of interpenetrating phenyl rings from neighboring rotors proximal to the event are significant for both **1A** and **1B**. In addition, 6-fold (C_6) benzene rotations in clathrate **1A** were found to be directly correlated to the rotation of the phenylene rotator.

Introduction

Progress in molecular and crystal engineering[1] and the development of methods to analyze solid-state dynamics[2] have converged to make feasible the design and characterization of crystalline nanodevices. The mechanical operations of several macroscopic objects have been emulated with elegantly designed molecules in solution[3] and on surfaces.[4] High density or crystalline solid devices with well-defined and controllable motions are significantly more interesting and challenging, as illustrated by recent experimental[5] and computational[6] research. These intriguing targets require structural elements that define a static frame of reference, which organize a set of highly mobile elements that respond to external stimuli. We have suggested the term "amphidynamic crystals" for rigid crystals with internal moving parts.[7] With that in mind, we seek to develop organic molecular crystals where each molecule incorporates a submolecular unit that undergoes rapid rotational motion.[8] Our design is inspired by macroscopic objects, such as gyroscopes and compasses. The function of a macroscopic gyroscope relies on the conservation of its angular momentum, while that of a compass operates on the orientation dependence of its magnetic

(1) (a) Desiraju, G. R. *J. Mol. Struct.* **2003**, *656*, 5. (b) Moulton, B.; Zaworotko, M. J. *Chem. Rev.* **2001**, *101*, 1629−1658. (c) Hollingsworth, M. D. *Science* **2002**, *295*, 2410−2413. (d) Kitagawa, S.; Kitaura, R.; Noro, S.-I. *Angew. Chem., Int. Ed.* **2004**, *43*, 2334−2375. (e) Friscic, T.; MacGillivray, L. R. *Z. Kristallogr.* **2005**, *220*, 351−363. (f) Wuest, J. D. *Chem. Commun.* **2005**, 5830−5837. (g) Ward, M. D. *Chem. Commun.* **2005**, 5838−5842. (h) Fyfe, M. C. T.; Stoddart, J. F. *Coord. Chem. Rev.* **1999**, *183*, 139−155.

(2) (a) Bürgi, H. B. *Annu. Rev. Phys. Chem.* **2000**, *51*, 275−296. (b) Dunitz, J. D.; Maverick, E. F.; Trueblood, K. N. *Angew. Chem., Int. Ed. Engl.* **1988**, *27*, 880−895. (c) Gavezzotti, A.; Simonetta, M. *Chem. Rev.* **1982**, *82*, 1−13. (d) Fyfe, C. A. *Solid-State NMR for Chemists*; CFC Press: Guelph, Ontario, 1983. (e) Lyerla, J. R.; Yannoni, C. S.; Fyfe, C. A. *Acc. Chem. Res.* **1982**, *15*, 208−216. (f) Blumich, B.; Spiess, H. W. *Angew. Chem., Int. Ed. Engl.* **1988**, *27*, 1655−1672. (g) Wendeler, M.; Fattah, J.; Twyman, J. M.; Edwards, A. J.; Dobson, C. M.; Heyes, S. J.; Prout, K. *J. Am. Chem. Soc.* **1997**, *119*, 9793−9803.

(3) (a) Mislow, K. *Chemtracts: Org. Chem.* **1988**, *2*, 151−174. (b) Balzani, C.; Gomez-Lopez, M.; Stoddart, J. F. *Acc. Chem. Res.* **1998**, *31*, 405−414. (c) Balzani, V.; Credi, A.; Raymo, F. M.; Stoddart, J. F. *Angew. Chem., Int. Ed.* **2000**, *39*, 3348−3391. (d) Feringa, B. L. *Acc. Chem. Res.* **2001**, *36*, 504−513. (e) Sauvage, J.-P. *Molecular Machines and Motors*; Springer-Verlag: New York, 2001; Vol. 99. (f) Stoddart, J. F. *Acc. Chem. Res.* **2001**, *36*, 410−411.

(4) (a) Fletcher, S. P.; Dumur, F.; Pollard, M. M.; Feringa, B. L. *Science* **2005**, *310*, 80−82. (b) Balzani, V.; Credi, A.; Venturi, M. *Molecular Devices and Machines − A Journey into the Nano World*; Wiley-VCH: Weinheim, Germany, 2003. (c) Sauvage, J.-P. *Molecular Machines and Motors*; Springer-Verlag: New York, 2001; Vol. 99. (d) Kelly, T. R.; De Silva, H.; Silva, R. A. *Nature* **1999**, *401*, 150−152. (e) Leigh, D. A.; Wong, J. K. Y.; Dehez, F.; Zerbetto, F. *Nature* **2003**, *242*, 174−179. (f) van Delden, R. A.; ter Wiel, M. K. J.; Pollard, M. M.; Vicario, J.; Koumura, N.; Feringa, B. L. *Nature* **2005**, *437*, 1337−1340. (g) Steuerman, D. W.; Tseng, H.-R.; Peters, A. J.; Flood, A. H.; Jeppesen, J. O.; Nielsen, K. A.; Stoddart, J. F.; Heath, J. R. *Angew. Chem., Int. Ed.* **2004**, *43*, 6486−6491. (h) Hernandez, R.; Tseng, H.-R.; Wong, J. W.; Stoddart, J. F.; Zink, J. I. *J. Am. Chem. Soc.* **2004**, *128*, 3370−3371. (i) Luo, Y.; Collier, C. P.; Jeppesen, J. O.; Nielsen, K. A.; DeIonno, E.; Ho, G.; Perkins, J.; Tseng, H.-R.; Yamamoto, T.; Stoddart, J. F.; Heath, J. R. *ChemPhysChem* **2002**, *3*, 519.

(5) (a) Karlen, S. D.; Garcia-Garibay, M. A. *Top. Curr. Chem.* **2006**, *262*, 179−227. (b) Khuong, T.-A. V.; Nuñez, J. E.; Godinez, C. E.; Garcia-Garibay, M. A. *Acc. Chem. Res.* **2006**, *39*, 413−422.

(6) (a) Baudry, J.; Smith, J. C. *J. Phys. Chem. B* **2005**, *109*, 20572−20578; (b) Baudry, J. *J. Am. Chem. Soc.* **2006**, *128*, 11088−11093.

10.1021/ja0637907 CCC: $37.00

Scheme 1

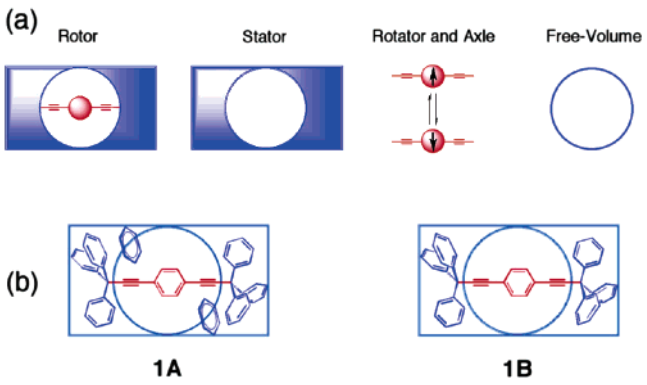

dipole energy. These devices are mechanically similar, both consist of a rotating or reorienting component, the rotator, and an encapsulating rigid frame, the stator,[9] which are linked together by a frictionless axle that passes through the center-of-mass of the rotator. Dynamic processes at the molecular level should be very different. Molecular gyroscopes with rotational barriers that are higher than the available thermal energy (*kT*) are expected to undergo random back and forth displacements between energy minima (site exchange) in steps that depend on the symmetry of their rotational axes.[8a] In contrast, molecular gyroscopes with barriers that are lower than thermal energy may approach the inertial rotary motion characteristic of the macroscopic objects. In our generalized nanoscale design (Scheme 1a), a molecular rotor consists of a central rotator, linked by two axially arranged acetylenes acting as a rotary axle, and two sterically bulky groups that act as a stator.

In Scheme 1, we use red to indicate dynamic components and blue to indicate the static ones. The unfilled region represents free volume. At the molecular level, gyroscopes and compasses may satisfy most of the mechanical requirements stated above for the macroscopic devises, yet we believe that their function in the crystalline state would rely on their order and collective behavior rather than on their independent action. These materials may be viewed of as composed of an infinite network of molecular gyroscopes or compasses, which are expected to have properties that arise from the collective behavior of the individual molecules. Emergent phenomena,[10] such as this, are an important intellectual driving force behind material science in general.

Free volume about the rotator is necessary for the function of both the macroscopic and the nanoscopic devices to prevent the rotators from experiencing friction with their environment (stator). This is a challenging design element that hinders the transfer of the mechanical properties of a single molecular device to a molecular assembly or infinite crystal lattice. Knowing that molecular crystals are formed upon the principle of close packing, it is conceptually difficult to maintain free volume in the solid state.[11,12] Relatively rigid and dumbbell-shaped structures such as those generalized in Scheme 1a have predictable packing structures with low densities that allow the rotation of the central group.[13] The orientation and distance between molecules is controlled by supramolecular stator−stator interactions. Variations in the structure of the stator have been used to achieve a variety of architectures, and variations in the symmetries of the rotator have been used to affect the magnitude of the barrier.[14] To introduce a permanent electric dipole, several polar substituents (fluoro, amino, nitro, cyano, etc.) have been appended to the rotator.[8f] Bulk materials with the properties of a macroscopic compass are particularly intriguing because they may provide access to nonlinear optical and electro-optical devices that can respond rapidly and reversibly to electromagnetic stimuli.[15]

The structures of molecular rotor **1** in the clathrate (**1A**) and desolvated (**1B**) forms are shown in Scheme 1b. The stator is comprised of two bulky trityl groups, and the rotator is a 1,4-dialkynylphenylene. The crystal structures of **1A** and **1B** are shown in Figure 1 for a 3 × 3 × 3 grid of molecular rotors, which is also shown in schematic form.

The benzene clathrate **1A** and the solvent-free form **1B** are structurally related by a first-order phase transition. Both structures belong to the space group $P\bar{1}$ (Figure 1) with coincident molecular and crystallographic inversion centers. Their unit cells are described with only one molecule of **1**, plus two additional benzene molecules in the case of **1A**. Molecular rotors in the benzene-clathrate **1A** pack in chains with their long axes roughly aligned along the *bc* diagonal (indicated in Figure 1). Infinite chains result from a well-known supramolecular synthon, known as a "trityl embrace,"[16] which consists of complementary face-to-edge interactions between trityl groups of adjacent molecules. Desolvation of **1A** by heating to ca. 120 °C results in the formation of **1B**, which can be selectively obtained by crystallization from methylene chloride. The structure of **1B** has different unit cell dimensions, but a packing topology similar to that of **1A** (Figure 1) with small changes in unit cell angles, a modest expansion in the *a*- and *b*-directions (7.4% and 8.0%, respectively), and a large 27.4% contraction along the *c*-axis. The space occupied by benzene dimers in clathrate **1A** is filled by trityl groups of adjacent molecules, which fill-in the space contiguous to their phenylene groups by

(7) Garcia-Garibay, M. A. *Proc. Natl. Acad. Sci. U.S.A.* **2005**, *102*, 10771−10776.
(8) (a) Karlen, S. D.; Ortiz, R.; Chapman, O. L.; Garcia-Garibay, M. A. *J. Am. Chem. Soc.* **2005**, *127*, 6554−6555. (b) Karlen, S. D.; Garcia-Garibay, M. A. *Chem. Commun.* **2005**, 189−191. (c) Karlen, S. D.; Khan, S. I.; Garcia-Garibay, M. A. *Cryst. Growth Des.* **2005**, *5*, 53−55. (d) Godinez, C. E.; Zepeda, G.; Mortko, C. J.; Dang, H.; Garcia-Garibay, M. A. *J. Org. Chem.* **2004**, *69*, 1652−1662. (e) Khuong, T.-A. V.; Zepeda, G.; Ruiz, G.; Khan, S. I.; Garcia-Garibay, M. A. *Cryst. Growth Des.* **2004**, *4*, 15−18. (f) Dominguez, Z.; Khuong, T.-A. V.; Dang, H.; Sanrame, C. N.; Nuñez, J. E.; Garcia-Garibay, M. A. *J. Am. Chem. Soc.* **2003**, *125*, 8827−8837. (g) Godinez, C. E.; Zepeda, G.; Garcia-Garibay, M. A. *J. Am. Chem. Soc.* **2002**, *124*, 4701−7707.
(9) We adopt here the definitions suggested in the following review: Kottas, G. S.; Clarke, L. I.; Horinek, D.; Michl, J. *Chem. Rev.* **2005**, *105*, 1281−1376.
(10) (a) Fromm, J. *The Emergence of Complexity*; Kassel University Press: Kassel, 2004. (b) Cox, D. L.; Pines, D. *MRS Bull.* **2005**, *30*, 425−432. (c) Laughlin, R. B.; Pines, D.; Schmalian, J.; Stojkovic, B. P.; Wolynes, P. *Proc. Natl. Acad. Sci. U.S.A.* **2000**, *97*, 32−37.
(11) (a) Kitaigorodskii, A. I. *Molecular Crystals and Molecules*; Academic Press: New York, 1973. (b) Vainshtein, B. K.; Fridkin, V. M.; Indenbom, V. L. *Structure of Crystals*; Springer-Verlag: Berlin, 1982; Vol. II.
(12) Recent success on the formation of free volume in crystals has been achieved by taking advantage of metal organic frameworks: (a) Yaghi, O. M.; O'Keeffe, M.; Ockwig, N. W.; Chae, H. K.; Eddaoudi, M.; Kim, J. *Nature* **2003**, *423*, 705−714. (b) Li, H.; Eddaoudi, M.; O'Keeffe, M.; Yaghi, M. *Nature* **1999**, *402*, 276−279. (c) O'Keeffe, M.; Eddaoudi, M.; Li, H.; Reineke, T.; Yaghi, O. M. *J. Solid State Chem.* **2000**, *152*, 3−120.
(13) (a) Dominguez, Z.; Dang, H.; Strouse, J.; Garcia-Garibay, M. A. *J. Am. Chem. Soc.* **2002**, *124*, 2398−2399. (b) Dominguez, Z.; Dang, H.; Strouse, J.; Garcia-Garibay, M. A. *J. Am. Chem. Soc.* **2002**, *124*, 7719−7727.
(14) Karlen, S. D.; Ortiz, R.; Chapman, O. L.; Garcia-Garibay, M. A. *J. Am. Chem. Soc.* **2005**, *127*, 6554−6555.
(15) (a) Weber, M. J. *Handbook of Optical Materials*; CRC Press: Boca Raton, FL, 2002. (b) Salech, B. E. A.; Teich, M. C. *Fundamentals of Photonics*; Wiley-Interscience: New York, 1991.
(16) (a) Scudder, M.; Dance, I. *J. Chem. Soc., Dalton Trans.* **1998**, 329−344. (b) Scudder, M.; Dance, I. *Dalton* **2000**, 2909−2915.

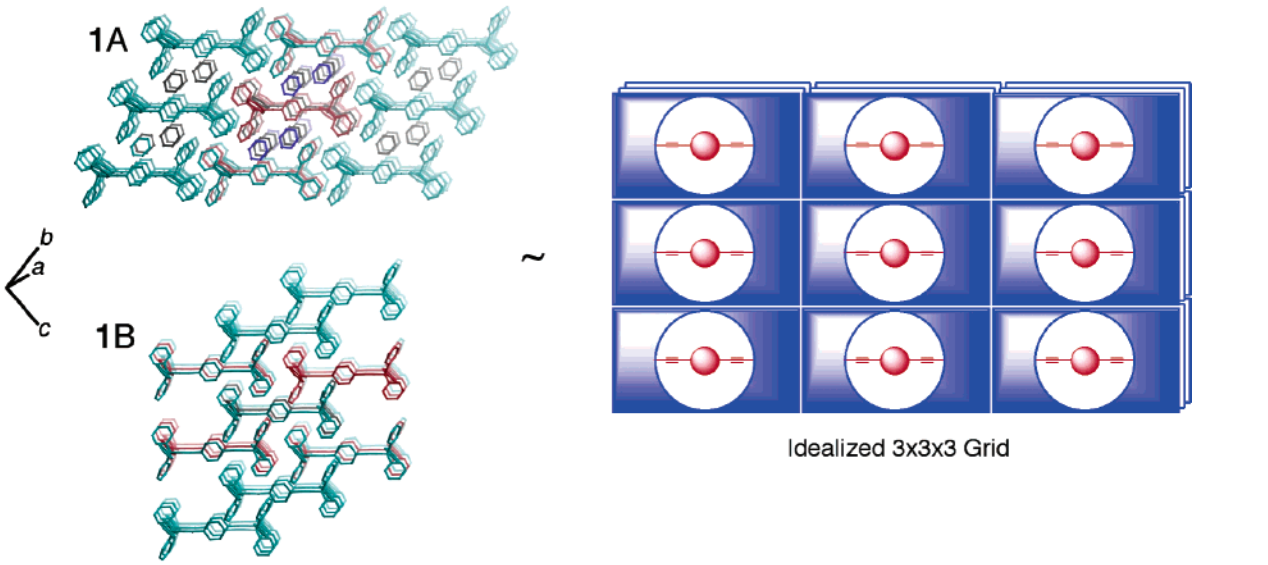

Figure 1. Crystal packing structures of the benzene clathrate **1A** (top) and desolvated form **1B** (bottom). Hydrogen atoms are not shown. See text for a description of the color scheme. The structures as shown are analogous to the schematic depiction of an idealized 3 × 3 × 3 lattice at right constituting a 27-rotor molecule assembly.

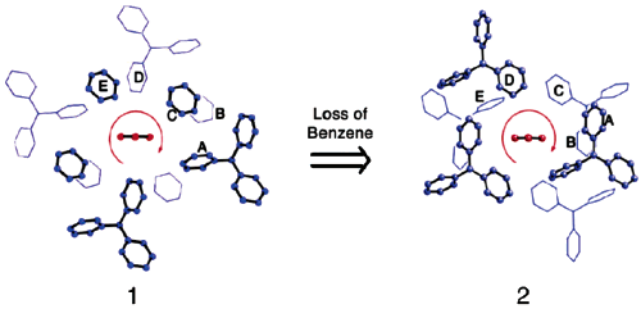

Figure 2. Supramolecular cages of clathrate **1A** (left) and desolvated crystals **1B**. The view is down the long axis of the central rotator with the trityl group removed for clarity. Only the trityl portions of the surrounding molecular rotors are shown. Ball and stick models indicate the groups that are closer to the viewer (above), and wire frame models indicate the groups that are farther away (below). All hydrogen atoms have been removed for clarity. Non-redundant rings are labeled A−E.

mutual interdigitation. Views of the close neighboring groups making up the local environments around the phenylene rotators, or "supramolecular cages", are illustrated in Figure 2. While the supramolecular cage of **1A** includes six benzene molecules and four interpenetrating phenyl groups, the one of **1B** consists of 10 phenyl rings from six surrounding trityl groups. It is interesting that both structures have 10 aromatic groups surrounding each phenylene rotator.

Compound **1** is the first and simplest test structure prepared in our group.[13] It has an open topology that exposes the rotator to close neighbors and potential solvent molecules in the crystal lattice. In fact, X-ray analyses of a benzene-containing clathrate[17] (**1A**) and desolvated crystal (**1B**) revealed close distances between the stator of one molecule and the rotator of another. In the former, close-contacts between the benzene molecules and rotator also exist. Experimentally, it was surprising that both the benzene clathrate (**1A**) and the desolvated crystal (**1B**) possessed rapidly rotating phenylenes despite having limited free volume. Experimental determinations carried out by VT

Scheme 2

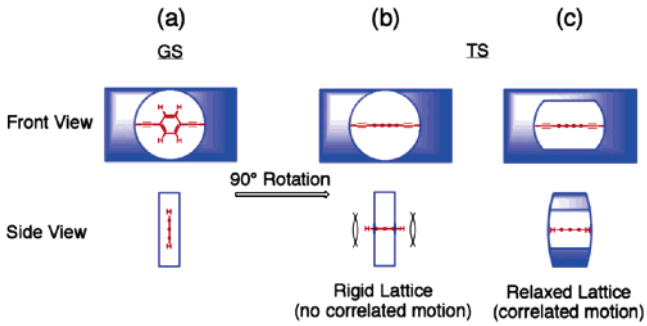

CPMAS, ^{13}C NMR, and ^{2}H NMR place the rotational motion of the rotator of **1A** and **1B** in the megahertz regime near room temperature, with barriers ranging in value from 12.8[13] kcal/mol for the former, and 11.3[18]−14.6[13] kcal/mol for the latter. Confirmation of these values and evidence for the interaction between polar rotators and external fields was obtained by dielectric loss measurements as a function of temperature and AC field frequency using fluoro-phenylene-substituted samples.[19] These solid-state barriers are much larger than the gas-phase values of ca. 0.1 kcal/mol,[20] but are low when one considers that the equilibrium structure of the environment in the crystal tends to fill the volume around the phenylene rotator, as illustrated in the ground-state representation in Scheme 2a. Having a flattened disk shape, the phenylene group 90° rotation should result in a transition state with a strong steric repulsion between the rotator and its environment (Scheme 2b). Calcula-

(17) Bernstein, J. *Polymorphism in Organic Chemistry*; Oxford University Press: Oxford, 2002.

(18) Karlen, S. D.; Garcia-Garibay, M. A. *Chem. Commun.* **2005**, 189−191.

(19) (a) Horansky, R. D.; Clarke, L. I.; Khuong, T.-A. V.; Jarowski, P. D.; Garcia-Garibay, M. A.; Price, J. C. *Phys. Rev. B* **2005**, *72*, 014302. (b) Horansky, R. D.; Clarke, L. I.; Winston, S. B.; Price, J. C.; Karlen, S. D.; Jarowski, P. D.; Santillan, R.; Garcia-Garibay, M. A. *Phys. Rev. B* **2006**, *74*, 054306.

(20) (a) Liberles, A.; Matlosz, B. *J. Org. Chem.* **1971**, *36*, 2710. (b) Saebo, S.; Almolof, J.; Boggs, J. E.; Stark, J. G. *J. Mol. Struct. (THEOCHEM)* **1989**, *200*, 361−373. (c) Sipachev, V. A.; Khaikin, L. S.; Grikina, O. E.; Nikitin, V. S.; Traettberg, M. *J. Mol. Struct.* **2000**, *523*, 1−22. (d) Abramenkov, A. V.; Almenningen, A.; Cyvin, S. J.; Jonvik, T.; Khaikin, L. S.; Rommingin, C.; Vilkov, L. V. *Acta Chem. Scand.* **1988**, *A42*, 674. (e) Sipachev, V. A.; Khaikin, L. S.; Grikina, O. E.; Nikitin, V. S.; Traettberg, M. *J. Mol. Struct.* **2000**, *523*, 1.

tions presented here indicate that a rigid lattice approximation is not a suitable model and that the observed low-energy barriers involve a large degree of correlated motions that change the shape of the local environment as the rotary event takes place (Scheme 2c).

The potential energy barriers for phenylene and fluorophenylene rotators were recently calculated with a relatively simple force field model having a central molecular gyroscope surrounded by its nearest neighboring molecules or portions thereof.[19] While these models needed many geometric constraints and were quite limited in their application, they gave potential barrier heights within 1−2 kcal/mol of the experimental free-energy barriers. In this paper, we improve the applicability of our previous work by increasing the size of the model and reducing the structural constraints so that structural changes can be monitored over greater distances. The 3 × 3 × 3 grids presented in Figure 1 are used to model the rotation of the centrally located rotator, which is driven about its dihedral angle. Structural analysis of the computational data with respect to the dihedral angle discloses the role of correlated motion on the energetics of rotation in these crystals.

Computational Methods

Model Molecular Assemblies. As a starting point to analyze the dynamics of molecular gyroscopes, and using a primarily phenomenological approach, we selected a model based on discrete molecular assemblies rather than a periodic boundary condition. While a periodic boundary condition would describe an infinite lattice with molecular rotations taking place in a coherent manner, the solid-state dynamics of **1A** and **1B** are best described in terms of a stochastic, 2-fold flipping process. In fact, experimental evidence shows that the population of rotating molecules of **1A** and **1B**, as well as other analogues, is a small and temperature-dependent fraction of the total, as expected for an event that has a relatively high-energy barrier.[13,19]

Calculations were performed using molecular mechanics with the force field MM3* as implemented in the program Macromodel.[21] Allinger's MM3 method is one of the most thoroughly tested mechanics methods for hydrocarbons.[22] Calculations began from initial coordinates taken directly from X-ray crystallographic data. Finite models **M-1A** and **M-1B**, which correspond to crystal structures **1A** and **1B**, respectively, were constructed with 3 × 3 × 3 grids of molecules (exactly as shown in Figure 1) that were excised from the infinite crystal lattice. The models in Figure 1 preserve the crystallographic inversion center of the space group $P\bar{1}$, with the center of the phenylene ring of the central molecule representing the inversion center of the entire cluster. **M-1A** includes 32 benzene molecules and 27 rotors (2598 atoms), while **M-1B** includes only the 27 rotors (2214 atoms). These systems are large enough to fully describe the local steric environment about the central rotator, which is directly in contact with four (**M-1A**) and six (**M-1B**) complete molecules. These groups constitute the supramolecular cage that is described in Figure 2. Additional molecular gyroscopes are included to extend the periphery of the model, where longer-range effects, between this supramolecular cage and groups beyond, may influence the rotational features. The vertical dimensions of **M-1A** and **M-1B** are about 15 Å, and the horizontal ones are somewhat longer. The structural changes up to these distances can be monitored as a function of rotator dihedral angle to assess the limits and distribution of correlated motion.

Model Constraints and Dihedral Driving Method. Some of the structural constraints of an infinite lattice can be modeled by applying artificial constraints to a subset of atoms to control the degrees of freedom restricted in the solid while avoiding artificial restrictions on motions that are likely to be allowed. Thus, four constraint sets have been tested against available experimental data: Constraint set I fixes all atoms (Figure 1, green and red rotors), except the six carbon and four hydrogen atoms of the central ring of the central rotator. The results of this constraint set represent the crystal modeled as a rigid medium and provide an upper energetic estimate for the rotational barrier in the absence of correlated motion of the lattice. Constraint set II assumes that translational movement of the molecules is unlikely and that the rotation of the trityl groups is restricted. To simulate these effects, the positions of the two methano trityl carbons (translational constraint) and the six ipso-carbons (rotational constraint) for each trityl group of each rotor are fixed (Figure 1, green, red, and black rotors). It should be noted that this constraint set allows for rotation about the axis passing through the ipso and para carbons of all six phenyl groups in the structure. Constraint set III includes only the translational constraint for the trityl groups (Figure 1, green, red, and black rotors), and constraint set IV is similar to constraint set II, except that the four (**M-1A**) or six (**M-1B**) trityl groups (red rotors) with contributing moieties to the supramolecular cage surrounding the central rotator are not constrained in any way. In case IV, the central rotor is completely unconstrained (black rotor). For the benzene clathrate **M-1A**, 24 of the 32 benzene molecules are unconstrained, including the 6 benzene molecules that encompass the supramolecular cage of the test rotator. However, there are 8 benzene molecules (Figure 1, blue benzenes) with all carbon atoms fixed in their original positions adjacent to the unfixed cage benzenes. These are necessary to stop the slippage of the cage benzenes during rotation. Each constraint set allows the relaxation of all other parameters in the molecular mechanics minimizations.

Scheme 3

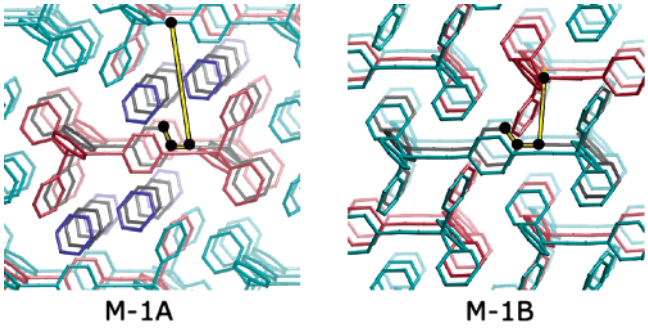

In the computational experiment, the rotator was driven 360° in increments of 10°, taking the value present in the crystal structures as the origin. We accomplished this by implementing the "dihedral driving" algorithm in macromodel.[23] Four atoms were chosen to define the dihedral angle to be driven. These differ slightly for **M-1A** and **M-1B** (Scheme 3), but in each case three of the atoms included were the sp carbon atom at the position of attachment to the rotator ring, and two sp^2 carbon atoms at the 1 and 2 positions of this ring. The fourth atom is a relatively stationary carbon atom of a nearby rotor molecule chosen on the basis of its proximity and coplanarity with the three other defining atoms. The atoms that define the dihedral angles are highlighted in Scheme 3 with black dots connected with a yellow line.

The constraints were applied using the default force constant of 100 kJ/mol·Å. During the dihedral driving run, the energy at each dihedral angle was minimized using the conjugate gradient PRCG method with an rms convergence threshold of 0.05 Å. The electrostatic cutoff was set to a 20 Å radius.

(21) Mohamadi, F.; Richards, N.; Guida, W. C.; Liskamp, R.; Lipton, M; Caufield, D.; Chang, T.; Hendrickson, T.; Still, W. *J. Comput. Chem.* **1990**, *11*, 440.
(22) Allinger, N. L.; Yuh, Y. H.; Lii, J.-H. *J. Am. Chem. Soc.* **1989**, *111*, 8551.
(23) Mohamadi, F.; Richards, N.; Guida, W. C.; Liskamp, R.; Lipton, M.; Caufield, C.; Chang, G.; Hendrickson, T.; Still, C. W. *J. Comput. Chem.* **1990**, *11*, 440.

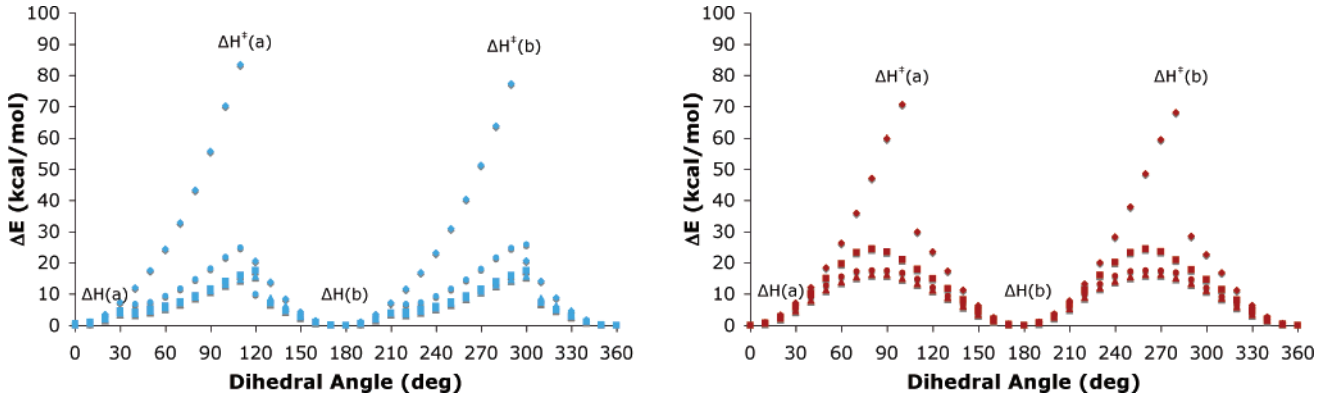

Figure 3. Rotational energy profile of clathrate **M-1A** (left) and desolvated **M-1B** (right) with constraint sets I (◆), II (■), III (●), and IV (▲).

Molecular Dynamics Calculations and Hysteresis. For constraint set IV, **M-1A** and **M-1B** dihedral drives were run in both directions to test for hysteresis. The **M-1B** runs were identical in each direction, but those of **M-1A** gave transition-state barriers displaced by 30° from each other, one direction giving a larger barrier. Thus, constrained molecular dynamics was performed on the clathrate for 100 ps with a 2 fs time step (298 K) and an equilibration time of 1 ps to generate 1000 sample structures to locate the global minima. This was done starting from the equilibrium X-ray structures for **M-1A** and **M-1B** and from the transition-state structures of **M-1B**, with a dihedral angle of 80° (see below), and **M-1A**, with a dihedral angle of 120° (see below). These dihedral angle values were constrained at these values (100 kJ/mol·deg). After the MD simulation, the lowest energy structures were, in turn, minimized. The energies of these structures were compared to those obtained directly from dihedral driving and were found to be a few kcal/mol higher in each case, for both the equilibrium and the transition states of **M-1A** and **M-1B**. This suggests that the profile obtained from dihedral driving is a good representation of the minimum energy rotational pathway.

Results and Discussion

Dependence on Constraint Model. The results for **M-1A** and **M-1B** with constraint sets I−IV are summarized in Figure 3.

The potential energy as a function of the phenylene dihedral angle from 0° to 360° in steps of 10° is plotted relative to the minimum, which is arbitrarily given a dihedral angle value of zero. The raw data for these profiles are given in the Supporting Information (SI 1). The rotational profiles for all four constraint sets have two isoenergetic minima [ΔH(a) = ΔH(b)] at 0° and 180°, and two essentially isoenergetic maxima [$\Delta H^{\ddagger}$(a) ≈ $\Delta H^{\ddagger}$(b)] separated by 180°. As expected from the symmetry of the rotator and the crystal lattice, the shape of the potential is periodic with respect to angular displacement with a period of 180°, but it is not symmetric with respect to the sign of rotation from the minima. The profiles for **M-1A** saw-tooth considerably, with the maxima much closer to one minimum than the other. The profiles of **M-1B** are closer to simple sinusoidal functions. The maxima for **M-1B** occur at 110° and 290°, while those for **M-1A** occur at 120° and 300°. As expected, the barrier heights are strongly dependent on the constraint set. Constraint set I results in rotational barriers of 80.4 and 69.3 kcal/mol for **M-1A** and **M-1B**, respectively. These barriers are much larger than the experimental values. Because lattice movements are restricted, rotation is made possible only by extreme distortion of the rotator, mostly through bending about the triple bonds (Csp^2−Csp bending). The barrier heights are significantly reduced when relaxation of the lattice is allowed for II−IV. The maxima for **M-1A** for constraint sets II, III, and IV are 25.3, 17.5, and15.5 kcal/mol, respectively. The corresponding barrier heights for **M-1B** are 24.4, 17.5, and 16.1 kcal/mol (for II, III, and IV). These values show a steady decrease in height with increasing lattice relaxation. The rotator does not distort significantly under these conditions. Constraint sets I and II for **M-1A** have maxima displaced by 10° from the dihedral angle values of the models using constraint sets III and IV. Similarly, the maxima for **M-1B** using constraints I and II are 20° displaced from constraints III and IV. The potential barriers using III and IV are close to the experimental free-energy values of 12−14 kcal/mol determined for both crystal structures.[7,13b,18] While the significance of this agreement cannot be assessed without entropic contributions, the improvement observed upon the systematic removal of structural constraints is significant and suggests the importance of local relaxation in the crystal lattice.

The energetic profile of a rigid lattice model represented by constraint set I should be determined by steric energy contributions. While electrostatic interactions may be also important, their contribution to the total energy in nonpolar aromatic crystals should be significantly smaller than the steric term, which has a repulsive contribution with steep distance dependence of $1/r$.[12] Further analysis of the energetic contributions to the rotational profile is provided in the Supporting Information (SI 2). A qualitative estimate of the effects of lattice relaxation may be obtained by taking the difference in barrier height between constraint sets I and IV. The structures at the corresponding maxima for **M-1A** and **M1-B** are stabilized by 64.9 and 53.2 kcal/mol, respectively.

Set IV has fewer artificial constraints than set III and provides rotational barriers that are closer to those obtained in the experiments. Because set II overestimates rotational barriers and set I is not at all realistic, set IV seemed optimal and was chosen to analyze the nature of the correlated motions in more detail.

Structural Analysis and Correlated Motion. In addition to lattice vibrations, which are not accounted for in our model, there are several molecular degrees of freedom that may contribute to the observed dynamic processes. These include in-plane rotation and small amplitude translations of benzene molecules in **1A**, and 2-fold rotation of the interpenetrating phenyl groups from neighboring molecules in the two crystal structures. These motions may change the size and shape of the supramolecular cage so that phenylene rotation may be correlated with them. The most energetically significant interac-

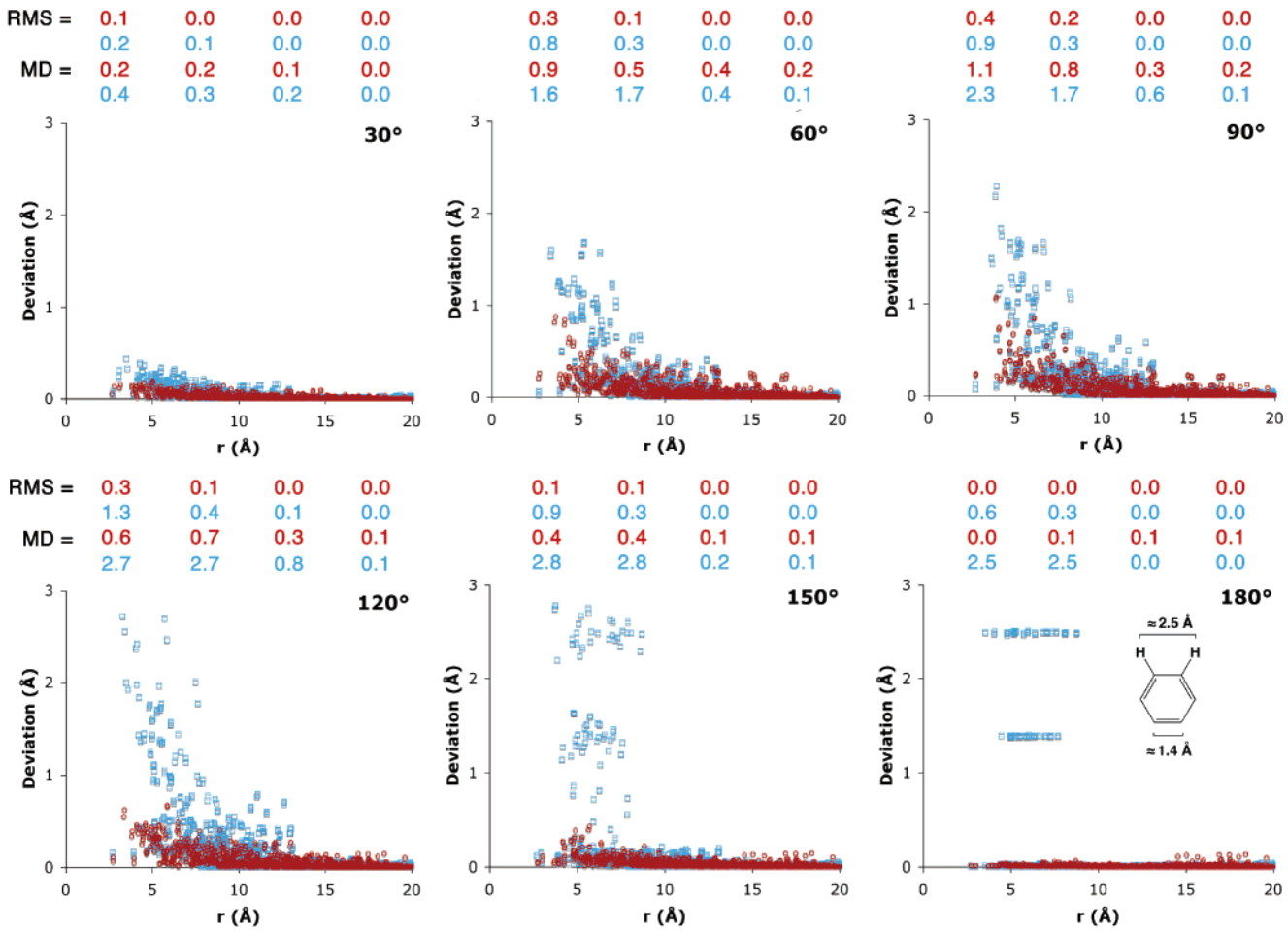

Figure 4. Positional displacement (deviation, Å) from the equilibrium structure (0°) versus distance (*r*, Å) from the center of the phenylene rotator in models of the benzene clathrate **M-1A** (blue □) and the desolvated form **M-1B** (red ○) at 30° increments. The root-mean-squared (rms) and maximum displacement (MD) are given for each data range (0−5, 5−10, 10−15, and 15−20 Å).

tions between the phenylene rotator and its environment should involve the groups that are part of the supramolecular cage (Figure 2); these are the most proximal to the rotary event. These interactions were analyzed by following the movement of all of the atoms in the models, except for the six carbon atoms and four hydrogen atoms of the central ring that are driven artificially to define the potential energy plot. A scatter plot of atomic displacements (deviation, Å) from the minimized equilibrium structure (0°) as a function of distance (*r*, Å) from the center of the rotator is plotted in Figure 4 for increments of 30° of the dihedral angle for **M-1A** in blue and for **M-1B** in red. The root-mean-squared displacement (rms) and the maximum displacement (MD) are included above the scatter plot for 5 Å distance intervals.

It should first be noted that the atomic positions in the equilibrium structure after minimization of the energy using constrain set IV remain nearly the same as those of the original X-ray structure, with rms deviation values of 0.1 Å for **M-1A** and 0.2 Å for **M-1B** (SI 3). There is a slight dependence of this deviation on the distance from the center of mass of the model, as the peripheries of these models are subject to greater freedom of movement up to a MD of ∼1 Å for both crystals. As shown in Figure 4, variation in atomic displacement relative to the calculated equilibrium structure at 0° is a strong function of the rotational angle of the central phenylene and the distance from this rotator; the largest displacement from the minimum

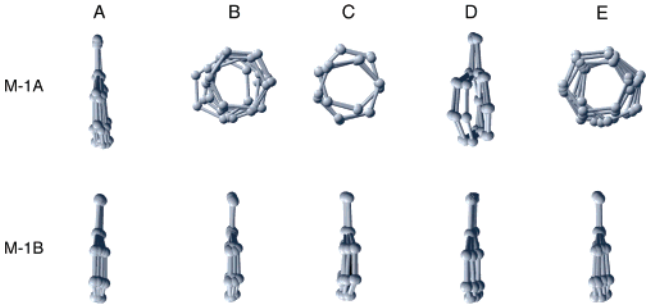

Figure 5. Overlaid structures at 30°, 60°, 90°, 120°, 150°, and 180° for rings A−E (defined in Figure 2) for **M-1A** and **M-1B**.

energy structure occurs at the rotational transition states. **M-1B** shows a steadily increasing number of significantly displaced atoms between the minimum (0°) and maximum (90°). This increase is most pronounced for atoms that are closest to the rotator, in the 0−5 Å data range. The maximum rms displacement for **M-1B** varies from 0.1 Å at 30° to 0.4 Å at the rotational transition state near 90°, where the maximum displacement is as large as 1.1 Å. There are no data below a distance of about 2.5 Å, because the atoms of the central phenylene ring are not included in the data set. The displacements are negligible above 20 Å. Atomic displacements at the rotational transition state in the 5−10 and 10−15 Å data ranges are small (rms = 0.2 and 0.0 Å, respectively). The rms displacement in the 15−20 range

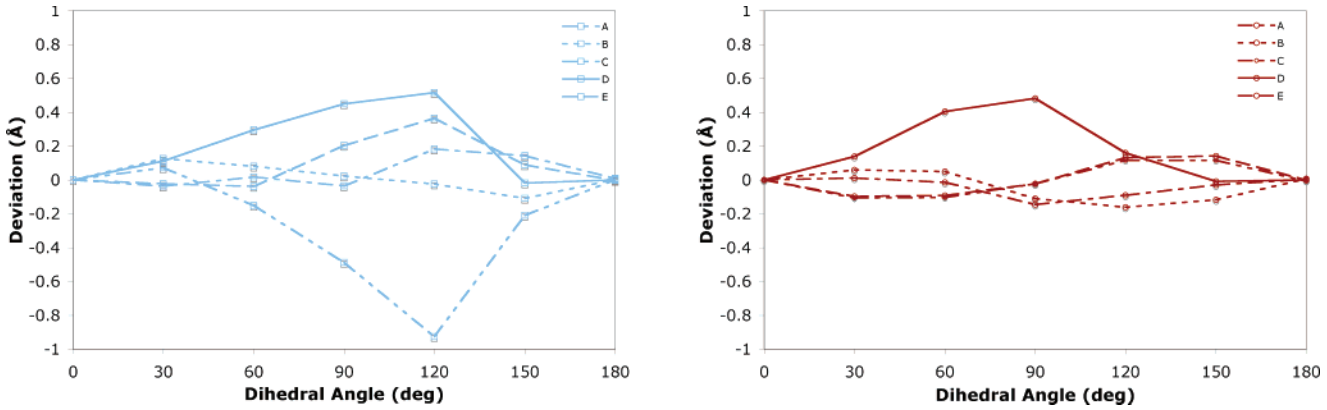

Figure 6. Displacement (deviation, Å) of the center of mass (six carbon atoms) of rings A−E for models of the benzene clathrate **M-1A** and the desolvated structure **M-1B** at 30°, 60°, 90°, 120°, 150°, and 180° with respect to the center of mass of the model at the minimum energy structures (0° and 180°).

is negligible (rms = 0.0 Å). Analysis of the MD values shows displacements of up to 0.3 Å in the 10−15 Å range and 0.2 in the 15−20 Å range, indicating that a few relatively distant atoms engage in significant structural excursions. At about 13 Å from the center of the central phenylene, there is an abrupt decrease in the number of data points showing a significant displacement. This is shown clearly at dihedral angles of 60°, 90°, and 120° and is an artifact of the model system, which has a horizontal dimension of 13−15 Å. While correlated displacements may continue beyond this point in the real lattice, the data suggest that structurally significant displacements may vanish beyond approximately 20 Å. Importantly, the central rotator is within 10 Å of all nearest neighboring rotators. The possibility of mechanically coupled rotator motions being mediated by lattice displacements has recently been discussed[19b] and is supported by this analysis. At a dihedral angle of 180°, the rms displacement drops close to zero for all data ranges as the equilibrium structure is reached (Figure 4). The same is true after a full 360° rotation (SI 2).

The results with **M-1A** convey quite different structural trends as compared to those with **M-1B**. Again, atomic displacements increase as a function of dihedral angle, but they are significantly greater in the 0−5 and 5−10 Å ranges than those found for **M-1B**. At a 30° dihedral, the rms displacements in these ranges are 0.2 and 0.1 Å, respectively, and the MDs are 0.4 and 0.3 Å, in the same order. At the maximum of 120°, these displacements are 1.3 and 0.4 Å, respectively. The 10−15 Å range has an rms displacement of 0.1 Å. The largest MD value at the rotational transition state is 2.7 Å both in the 0−5 and in the 5−10 Å ranges. The periphery of **M-1A** is about the same as for that of **M-1B**, and a similar discontinuity is found at a distance of approximately 13 Å. The most striking difference between **M-1A** and **M-1B** is that the former shows nonzero displacement at a dihedral angle of 180°. Starting at 90°, large displacements in the 0−5 distance range (1−2.5 Å) are found and continue through the transition state (120°) to the energy minimum at 180°. Over these dihedral angles, the data points begin with a relatively random pattern but then neatly cluster at two distinct values of 1.4 and 2.4 Å at 180°. The displaced data points correspond to benzene molecules in the supramolecular cage undergoing a degenerate 6-fold (C_6) rotation in concert with the 2-fold (C_2) rotator flipping motion. The displacement of the carbon atoms is smaller because they are closer to the axis of rotation and corresponds roughly to the length of a C=C double bond in benzene (1.4 Å). The associated hydrogen atoms are farther from the axis of rotation and are displaced by ca. 2.4 Å. Completing a full 360° rotational period of the central phenylene results (SI 4) in a second 60° step by the benzene molecules in the model, indicating that there is one C_6 rotation per 180° flip. These results are in line with the previous analysis of spectroscopic data where the correlated motion of the C_6 rotation and the C_2 rotation was compared to a slipping gear system.[13b] It is well known that C_6 rotation of benzene molecules in the solid state occurs with frequencies in the $10^{12}-10^{13}$ s^{-1} range,[24] which are much faster than the rate of phenylene flipping observed in these systems. Thus, although the data predict a 1:1 correlation of rotations, this does not mean that the C_6 rotation cannot occur without phenylene rotation. In fact, experimental results indicate that this coupling must be relatively week as benzene rotation takes place with rates $>10^8$ s^{-1} at temperatures where phenylene flipping occurs in the 10^3 s^{-1} range.[17b] Notably, the displaced data points include the atoms belonging to only five benzene rings, including both B and C (four benzenes) and one of the E rings. The other symmetry-related ring of E does not rotate, although its displacement behavior is nearly identical to its symmetric partner; at the critical point for rotation, the ring returns to its original position. We do not know the reasons for this outcome, but it may indicate the looseness of these correlations.

The correlated motions between the groups that make up the supramolecular cage and the central phenylene ring can also be illustrated by overlaying the structures of rings A−E (Figure 5).

The phenyl rings (A−E) of **M-1B** are relatively static as compared to those of **M-1A** (A and D). One can see that the displacement of the phenyl rings of adjacent trityl groups is best described as oscillations (librations) about the benzene-

(24) (a) Hoa, J.; Vodl, R. R.; Vold, R. L.; Etter, M. C. *J. Phys. Chem.* **1989**, *93*, 7618−7624. (b) Boden, N.; Clark, L. D.; Hanlos, S. M.; Mortimer, M. *Faraday Symp. Chem. Soc.* **1978**, 109.

(25) (a) Cholli, A. L.; Dumais, J. J.; Engel, A. K.; Jelinski, L. W. *Macromolecules* **1984**, *17*, 2399−2404. (b) Rice, D. M.; Wittebort, R. J.; Griffin, R. G.; Meirovich, E.; Stimson, E. R.; Meinwald, Y. C.; Freed, J. H.; Scheraga, H. A. *J. Am. Chem. Soc.* **1981**, *103*, 7707. (c) Rice, D. M.; Meinwald, Y. C.; Scheraga, H. A.; Griffin, R. G. *J. Am. Chem. Soc.* **1987**, *109*, 1636−1640. (d) Rice, D. M.; Blume, A.; Herzfeld, J.; Wittebort, R. J.; Huang, T. H.; Das Gupta, S. K.; Griffin, R. G. *Biomol. Stereodyn. Proc. Symp.* **1981**, *2*, 255−270. (e) Kamihira, M; Naito, A.; Tuzi, S.; Saito, H. *J. Phys. Chem. A* **1999**, *103*, 3356−3363. (f) Hiraoki, T.; Kogame, A.; Norio, N.; Akihiro, T. *J. Mol. Struct.* **1998**, *441*, 243−250. (g) Zhang, H.; Bryant, R. G. *Biophys. J.* **1997**, *72*, 372. (h) Naito, A.; Izuka, T.; Tuzi, S.; Price, W. S.; Hayamizu, K.; Saito, H. *J. Mol. Struct.* **1995**, *355*, 55−60.

trityl carbon−carbon bond. Interestingly, solid-state 2-fold flipping motions measured for the phenyl group of phenylalanine[25] in several crystal forms occur on the same time scale as the rotation of the 1,4-dialkynylbenzenes of **1A** and **1B**.[8] However, a correlated C_2 rotation of central phenylene with C_2 rotation in the neighboring phenyl groups is not observed in the calculation, nor in ^{2}H NMR experiments carried out with trityl-d_{30} isotopologues of the two crystal forms of **1**. A comparison of the transition-state energies for constraint set I to constraint set II (for **M-1B**) suggests that libration of the surrounding phenyl groups helps reduce the potential energy barrier of a hypothetical rigid lattice by 45 kcal/mol. A similar analysis for **M-1A** suggests that librations and benzene rotations reduce the corresponding barrier by 55.1 kcal/mol. Further structural analysis from constrain set IV shows that the rotation of the central phenylene in **M-1A** and **M-1B** is also aided by small displacements of the neighboring aromatic rings. The displacement of the center of mass for ring, A−E, in **M-1A** and **M-1B** from the center of the rotator is shown in Figure 6.

The translation of the rings as a function of the dihedral angle for both models occurs both away from (positive values) and toward (negative values) the center of the rotating phenylene. Displacements tend to be largest near the corresponding transition states. In the clathrate model **M-1A**, phenyl ring D is displaced away from the rotator, while benzene C is displaced toward it at the transition state of 120°. The solvent molecule is displaced by ca. 1 Å and the phenyl ring by ca. 0.5 Å. The direction of the displacement of other rings, such as benzene B, is dependent on the dihedral angle. Ring D is displaced ca. 0.5 Å away from the rotator at the transition state of 90°. Movements in this case can be also toward or away from the rotator depending on the dihedral angle. Rings A, B, C, and E switch direction at or near the transition state, indicating that the shape of the supramolecular cage is being molded continually to accommodate the rotator. A simple estimate of the energetic importance of these displacements at the transition state for **M-1B** takes the difference in barrier between constraint set II, which disallows translation of these rings, and IV, which does allow them. This difference is about 10 kcal/mol. A similar analysis is not possible for **M-1A** because the rotation of the benzene rings and the translation of these rings and those of the phenylenes are not able to be separated by comparison of constraint sets.

Conclusions

The rotational barriers for the two-fold flipping process of diethynyl phenylenes in crystals of the benzene clathrate **1A** and desolvated structure **1B** of 1,4-bis(3,3,3-triphenylpropynyl)-benzene have been calculated with molecular mechanics using large molecular assemblies constrained to model the crystal lattice. Potential barrier heights within a few kcal/mol of the experimental free-energy barriers are obtained when constraints are minimal. Estimates of the energetic consequences of correlated motion between the lattice and the rotator place this stabilization between 50 and 65 kcal/mol as compared to a rigid lattice approximation. For **M-1B**, the oscillatory motion (libration) associated with the rotational degree of freedom of the interdigitated phenyl rings of close neighboring molecules accounts for the majority of this stabilization, while displacements of the same phenyl groups account for a significantly smaller proportion. The structural changes that accompany these energetic effects have also been analyzed. Changes in atomic positions with respect to the equilibrium structure as a function of dihedral angle depend on the distance from the rotator. The displacements are larger in the model of the benzene clathrate **M-1A** as compared to those in the model for the solvent-free crystals **M-1B**. This is probably due to the greater freedom of the benzene molecules in the cage of the former. The 180° flipping motion of the rotator is correlated with a 60° rotation of the solvent molecules in **M-1A**, suggesting that phenylene rotation takes advantage of the well-documented rotation of benzene about its C_6 molecular axis, as in previous analysis of our spectroscopic data.[13b] The calculations also suggest that phenyl rings undergo oscillatory motions (librations) about their C_2 axis, but do not appear to rotate. All of these movements are also coupled to small translational displacement of the benzene and phenyl rings that move toward or away from the rotator to accommodate its intrusion along the rotational trajectories. Structural perturbations, measured in terms of atomic displacements, radiate outward from the rotary event, beyond the immediate environment of the supramolecular cages, to about 13 Å and possibly farther with relative magnitudes dependent on the distance from the rotator. Adjacent rotators within this distance may communicate through subtle structural changes in the lattice. The most important conclusion of this work is that, in the absence of large amounts of free volume, rotational motion in the solid state may be coupled to correlated motions in the crystal lattice. The present study illuminates many aspects of the rotational process, which are difficult to gauge experimentally. A better understanding of the factors that affect rotational motion in the solid state will be very useful in the design of molecular devices.

Acknowledgment. We are grateful to the National Science Foundation (DMR0307028 and DMR0605688) for financial support of this research. P.D.J. is grateful for the support of The American Chemical Society Organic Division Fellowship sponsored by Organic Reactions, Inc.

Supporting Information Available: Analysis of energetic contributions to the barriers and raw energy versus dihedral angle data. Frequency versus deviation bar graph of the calculated equilibrium structure as compared to the X-ray structure and scatter plot of atomic positions for equilibrium structure after 360° dihedral rotation. This material is available free of charge via the Internet at http://pubs.acs.org.

JA0637907